4. W. D. Hamilton, *J. Theor. Biol.* **7**, 1 (1964).
5. J. L. Brown, *Helping and Communal Breeding in Birds: Ecology and Evolution* (Princeton Univ. Press, Princeton, NJ, 1987).
6. M. Mesterton-Gibbons and L. A. Dugatkin, *Q. Rev. Biol.* **67**, 267 (1992).
7. D. H. Boucher, Ed., *The Biology of Mutualism: Ecology and Evolution* (Oxford Univ. Press, New York, 1985).
8. D. B. McDonald, *Anim. Behav.* **37**, 1007 (1989).
9. ———, *Behav. Ecol.* **4**, 297 (1993).
10. J. M. Trainer and D. B. McDonald, *Condor* **95**, 769 (1993).
11. Genotypes were assessed for 68 males, of which 28 were involved in one or more of 33 partnerships that were successful in attracting at least one female to a lek arena for dual-male dance display. Relatedness coefficients, $R_{I=1}$ $_{33}$, for each of 33 male partnerships were calculated from the four loci with the method of D. C. Queller and K. F. Goodnight [*Evolution* **43**, 258 (1989)]. With this method, relatedness coefficients can range from −1.0 to 1.0. A negative coefficient means that the individuals share fewer genes than the ambient level of sharing in the population. As with pedigree-based schemes, the expected relatedness among full siblings is 0.5. To assess the mean relatedness coefficient over all partnerships, the genotypes of the 40 unpartnered males were repeated 300 times as a background against which relatedness could be assessed. Only males were used for the analyses, because male and female Wright's inbreeding coefficient (F_{IS}) values differed slightly. All four loci conformed to Hardy-Weinberg expectations ($P \geq 0.25$).
12. R. R. Sokal and F. J. Rohlf, *Biometry* (Freeman, San Francisco, CA, 1981); two pairs of clutchmates had relatedness coefficients of 0.49 and 0.79, respectively. These individuals were at least half siblings and more likely full siblings.
13. Binomial test, $P = 0.36$ for 16 or more positive relatedness coefficients, on the assumption of an equal probability of positive or negative relatedness; $P < 0.05$ would require at least 22 positive coefficients.
14. D. B. McDonald, *Ethology* **94**, 31 (1993).
15. R. H. Wiley and K. Rabenold, *Evolution* **38**, 609 (1984).
16. For each of the measures of mating success, 2000 sets of eight values from the beta and predecessor columns of Table 3 were drawn randomly, with replacement. The drawing was constrained so that the paired value was neither self nor partner. Spearman rank correlation coefficients were calculated for each set of eight paired values. Of the 2000 sets drawn for female visitation, 23 coefficients (1.15%) exceeded the correlation coefficient between partners (0.71). Of the 2000 sets drawn for copulatory success, five coefficients (0.25%) exceeded the correlation coefficient between partners (0.83).
17. S. T. Emlen and P. H. Wrege, *Behav. Ecol. Sociobiol.* **23**, 305 (1988); C. Packer, D. A. Gilbert, A. E. Pusey, S. J. O'Brien, *Nature* **351**, 562 (1991); D. Queller, *Proc. Natl. Acad. Sci. U.S.A.* **86**, 3224 (1989); P. W. Sherman, J. U. M. Jarvis, R. D. Alexander, Eds., *The Biology of the Naked Mole Rat* (Princeton Univ. Press, Princeton, NJ, 1991).
18. J. D. Ligon, *Am. Nat.* **121**, 366 (1983); H.-U. Reyer, *Behav. Ecol. Sociobiol.* **6**, 219 (1980).
19. K. Sullivan, *Behaviour* **91**, 294 (1984); M. A. Elgar, *Biol. Rev.* **64**, 13 (1989); H. Kruuk, *The Social Badger* (Oxford Univ. Press, Oxford, 1989).
20. J. Sambrook, E. F. Fritsch, T. Maniatis, *Molecular Cloning: A Laboratory Manual* (Cold Spring Harbor Laboratory, Cold Spring Harbor, NY, 1989); D. Tautz, *Nucleic Acids Res.* **17**, 643 (1989); J. L. Weber and P. E. May, *Am. J. Hum. Genet.* **44**, 388 (1989).
21. Genomic DNA from long-tailed manakin and Florida scrub jay was digested with either Bam HI and Eco RI or Pst I and Sst I, as was the plasmid vector Puc 19. Genomic fragments between 200 and 700 base pairs (bp) were excised from agarose gels and cloned into Puc 19 to create size-selected genomic libraries for these two species. These libraries were screened simultaneously with radiolabeled $(CA)_n$ and $(CT)_n$ polynucleotides (Pharmacia). Positive clones were sequenced, and polymerase chain reaction (PCR) primers were developed for clones containing repeats with $n > 7$. Primer sequences for the four loci used in this study [three from the long-tailed manakin library (LTMR) and one from the Florida scrub jay library (SJR)] are as follows: SJR133, 5′-CATGCTTCATGGCTCAGTTCA-3′, and 5′-TGTGGGCAAGTGTGGGTGTAT-3′; LTMR6, 5′-GCCATGCCACAGGAGTGAGTC-3′, and 5′-AGTCATCTCCATCAAGG GCAT-3′; LTMR8, 5′-AATGACACCCCACATTCACTG-3′, and 5′-TGCCCAAATAGCAAAGGAACC-3′; LTMR15, 5′-CATTATTCCATAGTGCAAAGC-3′, and 5′-AACAGGTGCATCACTAAGCAG-3′. PCRs were performed in 25-μl volumes with the thermostable Taq-Polymerase, under conditions recommended by the supplier (Boehringer Mannheim, Indianapolis, IN) and 100 ng of template DNA. Thirty-five cycles of amplification were performed on a 9600 Perkin-Elmer thermocycler with 30 s at 94°C, 30 s at the annealing temperatures provided above, and 30 s at 72°C for each cycle. An initial 2-min denaturation at 94°C and a final extension of 7 min at 72°C were included. PCR products were mixed with 0.1% by volume glycerol dye, resolved on a 7% native acrylamide gel (30 cm by 45 cm), and visualized with ethidium bromide staining.
22. We thank R. L. Mumme, G. S. Wilkinson, V. Apanius, and two anonymous reviewers for incisive comments; D. C. Queller for providing the program for assessing relatedness and many useful tips; and K. Achey for technical assistance. D.B.M. thanks J. Gilardi, J. Stuckey, J. Stuckey, and many assistants for support in the field; the offices of V. Silvestre in Costa Rica for courteous assistance in securing permits; and Archbold Biological Station for logistical and scientific support. Supported by a grant from the National Science Foundation (D.B.M. and W.K.P.) and by grants from Earthwatch volunteers the National Geographic Society, and the Harry Frank Guggenheim Foundation (D.B.M.).

31 May 1994; accepted 15 August 1994

Molecular Maps of Red Cell Deformation: Hidden Elasticity and in Situ Connectivity

D. E. Discher,* N. Mohandas, E. A. Evans

Fluorescence-imaged micropipette aspiration was used to map redistribution of the proteins and lipids in highly extended human red blood cell membranes. Whereas the fluid bilayer distributed uniformly (±10 percent), the underlying, solidlike cytoskeleton of spectrin, actin, and protein 4.1 exhibited a steep gradient in density along the aspirated projection, which was reversible on release from deformation. Quantitation of the cytoskeletal protein density gradients showed that skeletal elasticity is well represented by a grafted polymer network with a ratio of surface dilation modulus to shear modulus of approximately 2:1. Fractionally mobile integral proteins, such as band 3, and highly mobile receptors, such as CD59 as well as glycophorin C in protein 4.1–deficient cells, appeared to be squeezed out of areas dense in the underlying network and enriched in areas of network dilation. This complementary segregation demonstrates patterning of cell surface components by cytoskeletal dilation.

Cell deformation is an integral feature of biological function even for passive capsules like red blood cells in the circulation. Such deformation can cause major rearrangements of structural proteins and lipids and thereby affect biological activity. The distributions of components in deformation provide significant clues to both strong structural connections and the susceptibility of those connections to gradients in chemical potential. A method has now been developed to map molecular distributions in well-defined states of deformation. Though this method was designed to be widely applicable to many types of cells, we used the human red blood cell as a prototypical system to demonstrate how extreme deformations act differentially on proteins and lipids in cell membranes supported by cytoskeletal networks. The results reveal a highly durable network that can sustain large chemical gradients with little relaxation over long periods (~30 min) of deformation.

The erythrocyte is a highly deformable membrane capsule with most of its mechanical features (with the exception of initial shape) largely decoupled from intracellular metabolism. Although many of the cell's component proteins, lipids, and carbohydrates have been identified (*1*), the functions of and physical connections between molecules in the assembled membrane during deformation are less clear. Key aspects of the deformability of the membrane arise from the underlying cytoskeleton (*2*), a prototypical assembly of structural proteins (*3*). Ultrastructural studies on membranes prepared for electron microscopy suggest, for example, that the in situ cytoskeleton is a highly organized, two-dimensional network of spectrin filaments interconnecting ~35,000 nodes or junctional complexes (*3*). The isolated junctional complexes consist primarily of three highly conserved and pervasive structural proteins: spectrin, ac-

D. E. Discher and N. Mohandas, Joint Graduate Group in Bioengineering, University of California at Berkeley and San Francisco, Berkeley, CA 94720, USA, and Life Sciences Division, Lawrence Berkeley Laboratory, Berkeley, CA 94720, USA.
E. A. Evans, Department of Pathology and Department of Physics, University of British Columbia, Vancouver, Canada V6T 1W5.
*To whom correspondence should be addressed.

tin, and protein 4.1 (*4*). The cytoskeletal assembly is thought to attach to the bilayer by association with integral membrane proteins, including band 3, a multispanning transmembrane protein (*5*) present at high surface density ($\sim 10^4$ molecules per square micrometer). Knowledge of the distributions of integral and peripheral membrane proteins relative to each other during large deformations of the cell is crucial to our understanding of in situ linkages.

To expose patterns of molecular components in response to forced deformation, we have developed the technique of fluorescence-imaged microdeformation (FIMD). Particular constituents were first fluorescently labeled either externally by standard methods (*6*, *7*) or internally by reversible permeabilization (*8*). Labeled components were expected to be either freely mobile in the lipid bilayer (lipid analogs and lipid-anchored proteins) or structurally integrated with the membrane skeleton (actin, spectrin, and band 3). Subsequent to labeling, an intact cell or a resealed cell "ghost" was aspirated into a micropipette (Fig. 1) (*9*). The extent of deformation was set by the projection length (L) inside the pipette, which was controlled by prior osmotic adjustment of the cell volume. Because cell surface area is maintained virtually constant by the small surface compressibility of the bilayer (*10*), pressurization of the cell ensured smooth membrane contours. After a period of time between several seconds and 30 min, a fluorescence image of the constituent distributions in the deformed state was collected. Before deformation, the constituent density fields were uniform (±10%).

To image the lipid bilayer distribution, we used the phospholipid analog fluorescein-phosphatidylethanolamine (FL-PE) and the lipophilic probe 1,1′-dioctadecyl-3,3,3′,3′-tetramethylindodicarbo-cyanine perchlorate [diIC_{18} (5)] (*6*). FL-PE distributed uniformly along the membrane projection as well as over the spherical segment outside the pipette (Fig. 1C), consistent with a mobility of >95% observed in fluorescence recovery after photobleach (FRAP) tests (*11*). Similar results were obtained with diIC_{18}. The bilayer component of the membrane responded to the deformation as a surface fluid with negligible change in area per lipid (*10*). Thus, the uniform surface density of lipid (Figs. 2A and 3A) enabled us to use the lipid intensity profiles for normalizing the fluorescence profiles of protein components independent of optical and geometric transformations.

In contrast to the uniform distribution of lipid along the aspirated projection of membrane, labeled components of the underlying cytoskeleton (*8*) exhibited strong gradients in density down the projection—decreasing toward the cap, although never vanishing. Both actin- (Fig. 1D) and spectrin-labeled red cell ghosts showed that the cytoskeleton deformed smoothly and axisymmetrically over the entire cell. Little intensity variation (<10%) was observed over most of the spherical sector outside the pipette. Incorporation of either fluorescein isothiocyanate (FITC)–labeled protein 4.1 or a fluorescein-labeled engineered spectrin-actin–binding domain of protein 4.1 in protein 4.1–deficient red cell ghosts gave similar patterns. The gradients in network density along the projection were relieved within seconds after the cell was released from aspiration (*9*), even after repetitive cycles of aspiration. The gradients persisted without relaxation over periods of $\gtrsim$30 min. Moreover, with increased projection length, the relative density of the network at the cap continuously decreased (Figs. 2B and 3A), demonstrating that spectrin filaments did not reach maximum extension (*12*). Together, these observations support

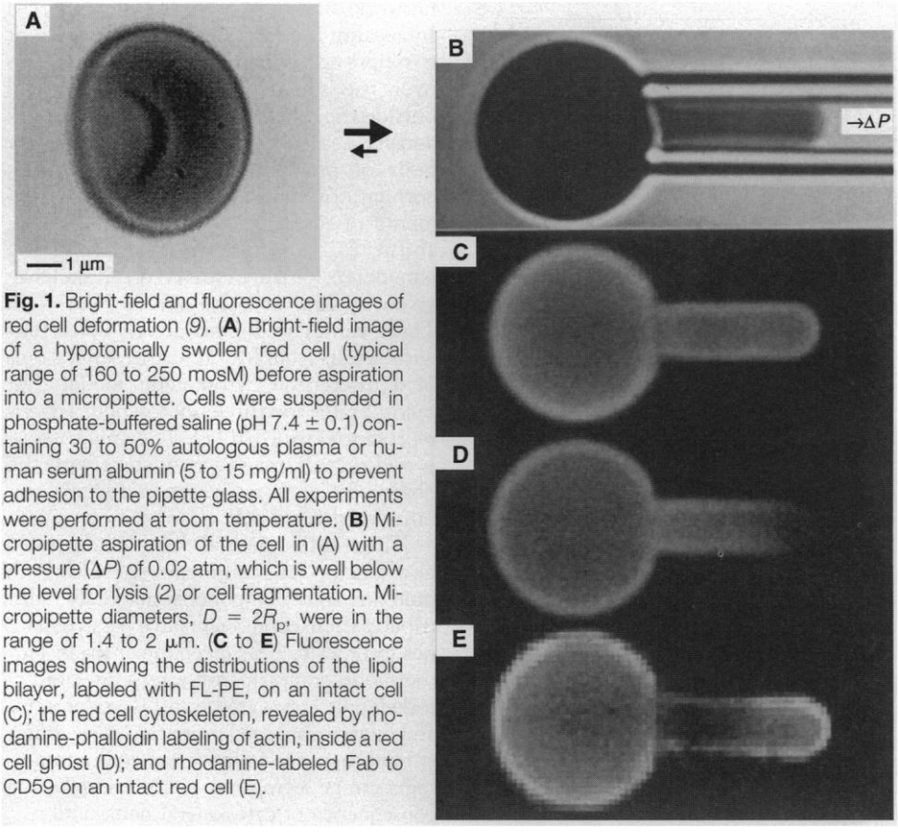

Fig. 1. Bright-field and fluorescence images of red cell deformation (*9*). (**A**) Bright-field image of a hypotonically swollen red cell (typical range of 160 to 250 mosM) before aspiration into a micropipette. Cells were suspended in phosphate-buffered saline (pH 7.4 ± 0.1) containing 30 to 50% autologous plasma or human serum albumin (5 to 15 mg/ml) to prevent adhesion to the pipette glass. All experiments were performed at room temperature. (**B**) Micropipette aspiration of the cell in (A) with a pressure (ΔP) of 0.02 atm, which is well below the level for lysis (*2*) or cell fragmentation. Micropipette diameters, $D = 2R_p$, were in the range of 1.4 to 2 μm. (**C** to **E**) Fluorescence images showing the distributions of the lipid bilayer, labeled with FL-PE, on an intact cell (C); the red cell cytoskeleton, revealed by rhodamine-phalloidin labeling of actin, inside a red cell ghost (D); and rhodamine-labeled Fab to CD59 on an intact red cell (E).

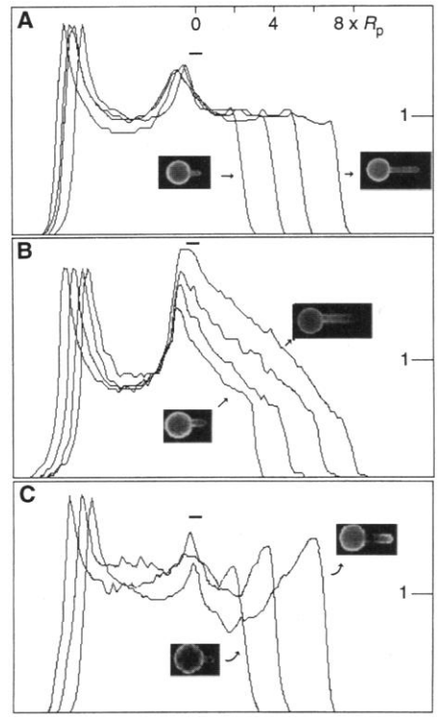

Fig. 2. Intensity sections of image types shown in Fig. 1. Density profiles along the projection were obtained from intensities integrated across a strip of width D bracketing the aspirated membrane projection. Thus, the surface area of the hemispherically capped cylinder illustrated in the image was a linear function of position along the axis. The small overbar marks the diffraction-limited position of the pipette entrance. (**A**) FL-PE sections superposed from four different cells. (**B**) Fluorescein-phalloidin–labeled actin sections superposed from four different cell ghosts. (**C**) Anti-CD59 Fab sections superposed from three different red cells.

the perception of the in situ network as a cohesive or solidlike structure.

Consistent with the fractional mobility detected by FRAP (*13*), our FIMD measurements of band 3 in intact cells (*7*) show density maps between those of the labeled cytoskeleton and the labeled bilayer (Fig. 4A). As with the labeled cytoskeleton, the band 3 gradient persisted for more than 30 min and was relieved on release from the pipette. Like the response of band 3, Fab labeling of glycophorin C on normal cells showed a decreasing density toward the cap (Fig. 4B), consistent with the proposal that this transmembrane glycoprotein and protein 4.1 form a link between the bilayer and the underlying cytoskeleton (*14*).

A different response was seen with membrane proteins not coupled directly to the cytoskeleton (*7*). The glycosylphosphatidylinositol-anchored protein CD59 (which lacks a transmembrane domain) concentrated progressively toward the tip of the projection (Figs. 1E and 2C). Two other mobile surface markers—a Texas red–labeled antibody bound to the fluorescein head group of FL-PE, as well as Fab-labeled glycophorin C on protein 4.1–deficient cells (Fig. 4B)—showed the same behavior. These countergradients in density of mobile surface components along the projection suggest that steric exclusion between the mobile species and large (*1*, *5*), dense cytoskeleton-linked species (such as band 3) results in component segregation (*15*). Under extreme aspiration, the tip of the aspirated projection could be forced to vesiculate from the cell body (which then resealed). The resulting vesicle was enriched severalfold in the uncoupled proteins and depleted of both band 3 and cytoskeletal components, consistent with the composition of red cell vesicles shed as a result of either Ca^{2+}-induced vesiculation, depletion of adenosine triphosphate, treatment with dimyristylphosphatidylcholine, or even long-term storage of blood (*16*). Similarly, the glycophorin C content of protein 4.1–deficient cells is reduced to one-third to one-tenth that of normal cells (*14*).

The red cell membrane skeleton thus supports large density gradients for protracted periods. This solidlike behavior resembles that of a cross-linked network of short polymer chains. Thus, with the application of theories for surface-grafted polymers (*17*) and building on earlier studies in red cell membrane mechanics (*2*, *18*), we have developed a parsimonious general model for cytoskeletal network elasticity (*19*). The model is based on the energetics of spectrin chain entropy restrictions and excluded volume interactions between network constituents. Given these actions, the least complicated form for the elastic energy density E_{net} (energy/area) is a sum of simple functions in both the local surface density and the surface shear:

$$E_{net} \approx (K/2)[1/\bar{\rho}^2 + (2/n)\bar{\rho}^n] + (\mu/2)(\lambda_1^2 + \lambda_2^2)$$

The geometric stretch ratios $\lambda_1 = L_1/L_0$ and $\lambda_2 = L_2/L_0$ and relative surface density $\bar{\rho} = 1/\lambda_1\lambda_2$ specify the deformation of a square element $L_0 \times L_0$ into a rectangle $L_1 \times L_2$. The terms in the energy represent entropy restrictions on chains tethered to the bilayer ($\sim 1/\bar{\rho}^2$), resistance to mass and charge condensation ($\sim\bar{\rho}^n$; $n > 0$), and reduction in chain entropy by stretch ($\sim\lambda_1^2 + \lambda_2^2$). For pressurization of a red cell discocyte into a well-defined axisymmetric form, deformations are completely represented by the spatial dependence of the relative density field, $\bar{\rho}$. Two important features characterize numerical predictions of minimum elastic energy with E_{net}, given the geometric data for pipette size, cell volume, cell area, and initial cell shape (*20*). (i) The gradient in density along the projection is determined principally by the ratio K/μ of network dilation to shear elasticities. (ii) Increasing the excluded volume exponent n suppresses both the density variations over the spherical segment of the cell outside the pipette and the rise in network density near the pipette entrance. On the basis of predicted density distributions, correlations (Fig. 3) with FIMD measurements of entrance and cap densities, $\bar{\rho}_e$ and $\bar{\rho}_c$ (or their ratio $\bar{\rho}_e/\bar{\rho}_c$), yield elastic parameters for the hidden red cell skeleton given by K/μ of $\sim 2{:}1$ and $1 \leq n < 2$. These values are quantitatively consistent with results from Monte Carlo simulations of a discretized cytoskeletal model that incorporates the three microscopic actions represented in E_{net} (*21*). The values ($K > \mu$ and $n > 0$) are also consistent with the observed elastic resilience and shape stability of the red cell.

The FIMD method has demonstrated how a composite cell membrane with both fluid and solid components markedly redistributes these components in a passive manner in order to bear mechanical loads. Furthermore, complementary responses of cytoskeletally connected transbilayer proteins and bilayer-anchored proteins expose different mechanisms by which membrane proteins can be segregated over the surface as a consequence of cytoskeletal deformation.

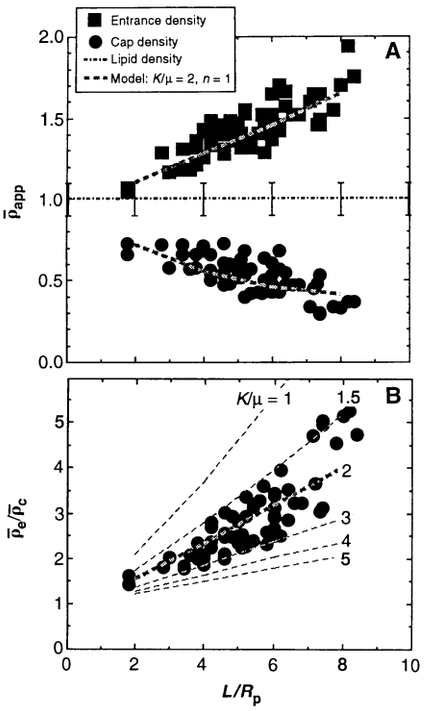

Fig. 3. FIMD measurements of actin density at the entrance ($\bar{\rho}_e$) and cap ($\bar{\rho}_c$) as a function of projection length. Only data with entrance and cap densities within 1.3 SD of binned averages, accounting for 70% of the cells tested, are shown. (**A**) Correlation of labeled actin densities with model parameters. The results for FL-PE lipid density along the projection are represented by averages of values taken at the midpoints of projections on >50 aspirated cells; the error bars represent a 10% coefficient of variation for the lipid profiles. (**B**) Predictions of the elastic deformation model for $n = 1$ and various values of network dilation modulus/shear modulus (K/μ) in relation to entrance: cap density ratio.

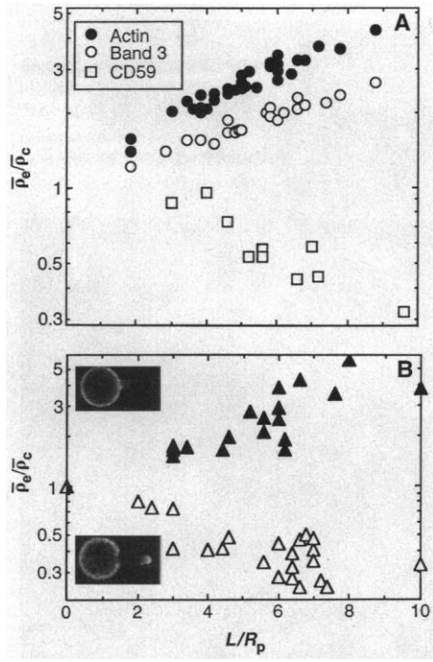

Fig. 4. Comparison of entrance:cap surface density ratios versus projection length. (**A**) Actin in ghosts, band 3 in both ghosts and intact cells, and CD59 on intact cells. (**B**) Glycophorin C on both normal (▲ and upper inset image) and protein 4.1–deficient (△ and lower inset image) red cells.

REFERENCES AND NOTES

1. S. R. Goodman *et al.*, *CRC Crit. Rev. Biochem.* **23**, 171 (1988); P. Ways and D. J. Hanahan, *J. Lipid Res.* **5**, 315 (1964); J. Viitala and J. Jarnefelt, *Trends Biochem. Sci.* **10**, 392 (1985).
2. E. A. Evans and R. Skalak, *Mechanics and Thermodynamics of Biomembranes* (CRC Press, Boca Raton, FL, 1980).
3. T. J. Byers and D. Branton, *Proc. Natl. Acad. Sci. U.S.A.* **82**, 6151 (1985).
4. D. M. Gilligan and V. Bennett, *Sem. Hematol.* **30**, 74 (1993); R. Debreuil *et al.*, *J. Cell Biol.* **105**, 2095 (1987); M. Spencer *et al.*, *Dev. Biol.* **139**, 279 (1990); M. D. Welch *et al.*, *Curr. Opin. Cell Biol.* **6**, 110 (1994).
5. N. Hamasaki and M. L. Jennings, Eds., *Anion Transport Protein of the Red Blood Cell Membrane* (Elsevier, New York, 1980); D. N. Wang, V. E. Sarabia, R. Reithmeier, W. Kuehlbrandt, *EMBO J.* **13**, 3230 (1994).
6. Fluorescent labels were obtained from Molecular Probes (Eugene, OR) unless otherwise noted. Membrane labeling with head group–conjugated fluorescein-phosphatidylethanolamine (FL-PE) (unsaturated, Avanti Polar Lipids, Alabaster, AL; saturated, Molecular Probes) was slightly modified from (*11*). Briefly, freshly washed cells (10 μl) were suspended in phosphate-buffered saline (90 μl) and FL-PE (dissolved in methanol) was added (1 μl to ~20 μM). The mixture was incubated for 30 min at 25°C. The lipid probe $diIC_{18}$ (*5*) was similarly intercalated.
7. Band 3 on intact red cells was labeled with eosin 5-maleimide (*13*) or fluorescein 5-maleimide and observed through either a fluorescein or longer wavelength filter set. The same type of response for band 3 was observed with cells in which both band 3 and actin were labeled with nonoverlapping fluorophores. Similar results were also obtained by labeling band 3 with a fluorescein isothiocyanate (FITC)–monoclonal Fab designated BRAC-18. CD59 on intact cells was labeled with a rhodamine-tagged monoclonal Fab. The purity of all Fabs was verified, and antibodies were centrifuged before use. For studies of glycophorin C, Fabs were generated from a monoclonal immunoglobulin G designated BRIC-10.
8. Red cells can be reversibly permeabilized by cold, hypotonic lysis so that fluorescent probes specific to internal structures can diffuse into the cell "ghost" and bind (*22*) [J. F. Hoffman, in *The Use of Resealed Erythrocytes as Carriers and Bioreactors*, M. Magnani and J. R. DeLoach, Eds. (Plenum, New York, 1992), pp. 1–15; M. D. Scott *et al.*, *J. Lab. Clin. Med.* **115**, 470 (1990)]. Labeling of cytoskeletal actin with fluorescein- or rhodamine-phalloidin was accomplished by first air-drying 2 to 5 μl of phalloidin at a concentration of 1 mg/ml in methanol and then redissolving it in 20 to 50 μl of cold lysis buffer [7.5 mM sodium phosphate (pH 7.4 ± 0.1)]. Cold, packed red cells (5 μl) were added and, after 5 min, the suspension was adjusted to 100 mM KCl, 1 mM $MgCl_2$, and 0.1 mM dithiothreitol and incubated at 37°C for 20 to 60 min. Mechanical properties of the resealed membrane were not altered by the labeling procedure, as evaluated by both micropipette aspiration and ektacytometry. A concentration-dependent edge brightness indicated an apparent in situ dissociation constant of $\sim 3 \times 10^{-7}$ M, slightly less than in vitro assays. None of the protein solutions fluorescently labeled unlysed cells. Protein 4.1 was purified and labeled by previously described methods [J. M. Tyler, W. R. Hargreaves, D. Branton, *Proc. Natl. Acad. Sci. U.S.A.* **76**, 5192 (1979); A. Podgorski and D. Elbaum, *Biochemistry* **24**, 7871 (1985)] and stored at 0.25 mg/ml in 50 mM KCl, 10 mM sodium phosphate (pH 7.4), 0.2 mM dithiothreitol, and 0.5 mM phenylmethylsulfonyl fluoride. Protein 4.1–deficient cells were labeled by a process similar to that for phalloidin. Iodoacetimido-5-fluorescein was conjugated to a recombinant glutathione-S-transferase fusion protein containing the spectrin-actin–binding domain of protein 4.1 (*23*). Incorporation of protein 4.1 or the recombinant spectrin-actin–binding domain has been shown to normalize the mechanical strength of protein 4.1–deficient membranes (*22*, *23*). Polyclonal immunoglobulin G antibodies to the α-II(46) domain of α-spectrin were subjected to proteolysis to yield Fab fragments, which were then labeled with FITC. Incorporation provided a view of the gradient similar to that of phalloidin-labeled actin and labeling of protein 4.1. Ektacytometry has shown that anti-spectrin Fabs do not alter membrane deformability [K. Nakashima and E. Beutler, *Proc. Natl. Acad. Sci. U.S.A.* **75**, 3823 (1978)].
9. The micropipette system is based on previous descriptions [E. A. Evans, *Methods Enzymol.* **173**, 3 (1989)]. In the present studies [D. E. Discher, thesis, University of California at Berkeley and San Francisco (1993)], a conventional Nikon Diaphot was fitted with a standard video camera and also with a liquid N_2–cooled charge-coupled device camera (CH-260; Photometrics, Tucson, AZ) for accurate quantitation of very low level fluorescence [Y. Hiraoka, J. W. Sedat, D. A. Agard, *Science* **238**, 36 (1987)]. To collect light from the full depth of the fluorescing membrane cylinder, we used an objective lens with a depth of focus similar to the pipette diameter (Zeiss Neofluar; 40×, 0.75 numerical aperture). The interval of aspiration to the deformed state was varied from <1 s up to 5 min, and image collection ranged from 100 ms to 10 s; neither variable had a discernible effect. Similar images were obtained with both higher and lower power objectives. For fluorescein, excitation was at 480 ± 15 nm, dichroic at 510 nm, and emission at 535 ± 20 nm. For longer wavelengths, excitation was at 560 ± 20 nm, dichroic at 595 nm, and emission at 655 ± 20 nm. Although the aspiration process was fully reversible under brightfield illumination, prolonged excitation of fluorescence invariably resulted in photofixation, which could be demonstrated by the cell partially retaining its aspirated form and density gradient after expulsion from the micropipette.
10. E. A. Evans and D. Needham, *J. Phys. Chem.* **91**, 4219 (1987).
11. J. A. Bloom and W. W. Webb, *Biophys. J.* **42**, 295 (1983); D. Golan *et al.*, *J. Cell Biol.* **103**, 819 (1986).
12. From (*3*), the distance between nodes is ~76 nm and the spectrin filament contour length is ~200 nm. The minimum relative density of an intact network is given by the squared ratio of these lengths, $\bar{\rho}_c \approx 0.14$.
13. D. Golan and W. Veatch, *Proc. Natl. Acad. Sci. U.S.A.* **77**, 2537 (1980); A. Tsuji and S. Ohnishi, *Biochemistry* **25**, 6133 (1986).
14. J. C. Pinder *et al.*, *Blood* **82**, 3482 (1993); M. Reid *et al.*, *ibid.* **75**, 2229 (1990).
15. On the basis of excluded area interactions, a simplistic quantitative treatment of the complementarity shown in Fig. 4 leads to an estimate of the areal fraction occupied by coupled integral proteins such as band 3 on the nascent membrane of between 25 and 55%.
16. C. Hagelberg and D. Allan, *Biochem. J.* **271**, 831 (1990).
17. P. G. deGennes, *Scaling Concepts in Polymer Physics* (Cornell Univ. Press, Ithaca, NY, 1988).
18. B. T. Stokke, A. Mikkelson, A. Elgsaeter, *J. Theor. Biol.* **123**, 205 (1986).
19. N. Mohandas and E. A. Evans, *Annu. Rev. Biophys. Biomol. Struct.* **23**, 787 (1994).
20. The reference shape for the calculations was a discocyte (*2*); results changed little with both the variations expected in cell geometry and the range of pipette sizes. The pipette radius, R_p, was 1 μm, and relative to the cell-sphered radius R_o, $R_o/R_p = 3$.
21. D. H. Boal, *Biophys. J.* **67**, 521 (1994).
22. Y. Takakuwa *et al.*, *J. Clin. Invest.* **78**, 80 (1986).
23. D. Discher, M. Parra, J. G. Conboy, N. Mohandas, *J. Biol. Chem.* **267**, 7186 (1993).

24. We thank A. Leung for technical assistance. D. Anstee (International Blood Group Reference Laboratory, Bristol, UK) provided BRAC-18 and BRIC-10. S. Test (Children's Hospital of Oakland Research Institute, Oakland, CA) provided rhodamine-tagged monoclonal Fab. S. Marchesi (Yale University) provided antispectrin. Supported in part by Department of Energy equipment funds and by NIH grants P01 DK32094-09 and R01 HL31579-13. N.M. has also been supported by NIH grant R01 DK26263-15.

31 May 1994; accepted 13 September 1994

Identification of Two GTP-Binding Proteins in the Chloroplast Protein Import Machinery

Felix Kessler, Günter Blobel, Hitesh A. Patel, Danny J. Schnell*

Two of four proteins that associated with translocation intermediates during protein import across the outer chloroplast envelope membrane were identified as guanosine triphosphate (GTP)–binding proteins. Both proteins are integral membrane proteins of the outer chloroplast membrane, and both are partially exposed on the chloroplast surface where they were accessible to thermolysin digestion. Engagement of the outer membrane's import machinery by an import substrate was inhibited by slowly hydrolyzable or nonhydrolyzable GTP analogs. Thus, these GTP-binding proteins may function in protein import into chloroplasts.

At least six distinct chloroplast envelope proteins are specifically engaged by a protein import substrate during its translocation across the two membranes of the envelope in an in vitro chloroplast import system (*1*). These proteins, referred to as IAPs (import intermediate–associated proteins), coisolated specifically and in apparently stoichiometric amounts with tagged import intermediates after detergent solubilization of an envelope subfraction of chloroplasts. A subset of four of these IAPs, referred to as early IAPs, are specifically engaged by early import intermediates and, therefore, are proposed to represent components of the outer membrane (OM) import machinery (*1*).

We have characterized two of these early IAPs, IAP34 and IAP86. These two proteins are indeed integral proteins of the outer chloroplast membrane, and both pro-

F. Kessler and G. Blobel, Laboratory of Cell Biology, Howard Hughes Medical Institute, The Rockefeller University, New York, NY 10021, USA.
H. A. Patel and D. J. Schnell, Department of Biological Sciences, Rutgers, The State University of New Jersey, Newark, NJ 07102, USA.

*To whom correspondence should be addressed.